ACS OMEGA

http://pubs.acs.org/journal/acsodf

Article

Well-Designed Au Nanorod-Doped Cu_2O Core–Shell Nanocube-Embedded Reduced Graphene Oxide Composite for Efficient Removal of a Water Pollutant Dye

Hansa Mahajan, Shiva Kumar Arumugasamy, Atanu Panda, Venkateswarlu Sada,* Minyoung Yoon,* and Kyusik Yun*

Cite This: *ACS Omega* 2020, 5, 24799–24810

Read Online

ACCESS | Metrics & More | Article Recommendations | Supporting Information

ABSTRACT: To ensure environmental safety, the removal of organic pollutants has gained increasing attention globally. We have synthesized uniform Au nanorod (NR)-doped Cu_2O core–shell nanocubes (CSNCs) via a seed-mediated route embedded on the surface of rGO sheets. The Au NRs@Cu_2O/rGO nanocomposite was characterized using various techniques such as transmission electron microscopy (TEM), atomic force microscopy (AFM), X-ray diffraction (XRD), X-ray photoelectron spectroscopy (XPS), and Fourier-transform infrared (FT-IR) and Raman spectroscopies. The scanning TEM-energy-dispersive spectroscopy (STEM-EDS) elemental mapping of the AuNRs@Cu_2O/rGO nanocomposite indicates that the Au NR (40 nm) is fully covered with the Cu_2O particles (~145 nm) as a shell. N_2 gas sorption analysis shows that the specific surface area of the composite is 205.5 m^2/g with a mesoporous character. Moreover, incorporation of Au NRs@Cu_2O CSNCs increases the nanogaps around the nanoparticles and suppresses the stacking/bundling of rGO, which significantly influences the pore size and increase the surface area. A batch adsorption experiment was carried out under various parameters, such as the effect of pH, contact time, temperature, initial dye concentration, and adsorbent dosage, for the removal of methylene blue (MB) in aqueous solution. The high surface area and mesoporosity can cause the adsorption capacity to reach equilibrium within 20 min with a 99.8% removal efficiency. Both kinetic and isotherm data were obtained and fitted very well with the pseudo-second-order kinetic and Langmuir isotherm model. The Langmuir isotherm revealed an excellent dye sorption capacity of 243.9 mg/g at 298 K. Moreover, after five adsorption cycles, the dye removal efficiency decreased from 99 to 86%. This novel route paves a new path for heterogeneous adsorbent synthesis, which is useful for catalysis and electrochemical applications.

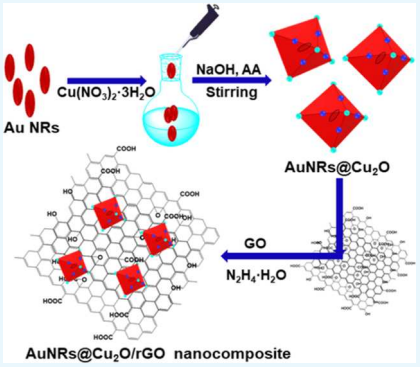

INTRODUCTION

The rapid growth of chemical industries can cause serious aquatic pollution, due to inferior standards, copious hazardous materials (heavy metals, oils, organic molecules, etc.) entering the environment water system.[1] Among them, organic dyes are widely used in various industries, and annually nearly 210 000 tons of dyes are discarded.[2] Especially, methylene blue (MB), a heterocyclic aromatic cationic dye, is one of the popularly used substances for the manufacturing of textiles, wool, and pigmentation of papers and cosmetics.[3,4] The dye is stable against biodegradation and can prevent the sunlight reaction with water systems, which inhibits the growth of biota, due to depilation of photosynthetic activity, and causes biological imbalance.[5] MB can cause harmful effects such as vomiting, increased heart rate, diarrhea, shock, cyanosis, quadriplegia, tissue necrosis, etc.[6,7] Therefore, the removal of MB is of utmost importance. Moreover, several techniques have been extensively reported, such as membrane filtration, electrochemical method, flotation, coagulation, chemical oxidation, ion exchange, and adsorption.[8−10] Among all of the physiochemical methods, adsorption is considered as one of the most eco-friendly, easy-to-operate methods, generating a negligible amount of secondary waste and recycling adsorbents.[11] Moreover, several adsorbents such as activated carbons, graphene, biochar, agricultural waste, clay, polymers, and silicates are used for the removal of MB.[12−16] Nevertheless, some limitations such as low adsorption capacity, poor stability, and low selectivity restrict their wide applications. Recently, nanostructured absorbents, such as nanoparticles (Fe_3O_4, TiO_2, CeO_2, ZnO, $ZnSnO_3$, C_3N_4, and Cu_2O), nanorods, and nanofibers, have attracted considerable attention for the removal of diverse toxic dyes from wastewater,[17−19] owing to their promotion of charge separation, smaller size, interparticle interaction affinity, and

Received: July 21, 2020
Accepted: September 2, 2020
Published: September 16, 2020

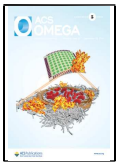

https://dx.doi.org/10.1021/acsomega.0c03487
ACS Omega 2020, 5, 24799–24810

high surface reactivity.[20,21] Among the various available metal oxides, Cu_2O is one of the highly used adsorbents, owing to its eco-friendly nature, low cost, mechanical strength, and good porosity.[22,23] However, bare Cu_2O has some demerits such as poor surface reactivity and less charge transfer kinetics. It is also known that the incorporation of a second phase such as Au nanoparticles may enhance the reactivity and thermal stability of a composite material.[24] In the literature, several studies have reported that the Au nanoparticle-doped Cu_2O system has been applied for the photodegradation of dyes.[25,26] However, very few reports illustrate Cu_2O applied as an adsorbent for the removal of dyes.[27] Nevertheless, the adsorption capacity and reactivity of bare Cu_2O are very poor. Therefore, it is still a challenge to synthesize highly efficient nanomaterials for the complete removal of hazardous dyes. Graphene oxide is considered as one of the most reactive, high surface area two-dimensional (2D) material.[28] However, graphene oxide (GO) also has some disadvantages such as high aggregation behavior and stack-forming.[29,30] To overcome all of the above drawbacks, a nanostructure with a high specific surface area and a highly reactive surface is an unmet demand. To the best of our knowledge, for the first time, we have developed a AuNRs@Cu_2O-embedded reduced graphene oxide (rGO) composite for the removal of organic methylene blue.

Herein, we present a facile method for the synthesis of a uniformly dispersed Au nanorod-doped Cu_2O CSNC-embedded rGO composite (AuNRs@Cu_2O/rGO). Interestingly, our AuNRs@Cu_2O/rGO shows a higher surface area (205.5 m^2/g) than pristine GO (9.7 m^2/g). Due to the incorporation of nanoparticles, the nanogaps around the nanoparticles can be increased, which can tune the pore size and increase the surface area.[22] The AuNRs@Cu_2O/rGO nanocomposite was well characterized using atomic force microscopy (AFM), transmission electron microscopy (TEM), energy-dispersive spectroscopy (EDS), X-ray photoelectron spectroscopy (XPS), Raman spectroscopy, etc. Owing to the high surface area, the AuNRs@Cu_2O/rGO nanocomposite exhibited a high MB adsorption capacity (243.9 mg/g) for removal from water. The effects of various parameters including pH, contact time, temperature, and dosage were studied. A detailed mechanism for dye removal is also provided. This composite is a newly emerging nanocomposite material with its characteristic structure that enables it to interact effectively with organic molecules. Finally, we have synthesized the AuNRs@Cu_2O/rGO alloy composite for multiple application purposes, such as photochemical, electrochemical, and water treatment. We first tested the dye adsorption behavior of the AuNRs@Cu_2O/rGO alloy composite, which was shown to be excellent (Scheme 1). Further applications, including photochemical and electrochemical applications, are now in progress.

RESULTS AND DISCUSSION

Structural Characterization. The morphology and structure of the Au NRs, AuNRs@Cu_2O CSNCs, GO, and the AuNRs@Cu_2O/rGO nanocomposite was analyzed using AFM, TEM, and EDS techniques. The AFM image reveals that the bare Au NRs are uniform in size and well dispersed (Figure 1a,b). The GO sheets appeared as a stacked two-dimensional (2D) structure (green arrows) (Figure 1c) with a thickness of 0.6−1.3 nm and size around 400−550 nm. The AFM and 3D AFM images of the composite indicate that the AuNRs@Cu_2O CSNCs (blue arrow) are well embedded onto the surface of the rGO sheet, which is also supported by the line profile image (Figure 1d−f). The line profile clearly shows the presence of humps, which implies that the composition is a mixture of AuNRs@Cu_2O CSNCs and the rGO sheet. This result was further confirmed by TEM and EDS analyses.

Scheme 1. Synthesis Process of the AuNRs@Cu_2O/rGO Nanocomposite

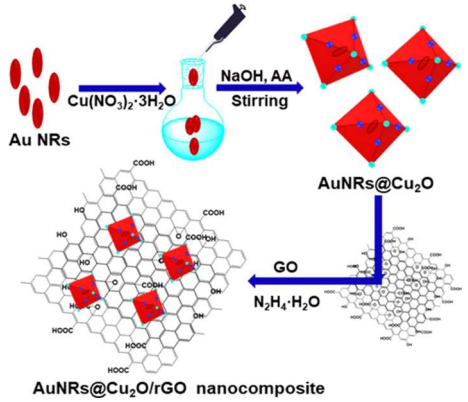

The TEM image shows the uniform dispersibility of the Au NRs with a length and width of 40 and 20 nm, respectively (Figure 2a). In addition, the core−shell structure of AuNRs@Cu_2O CSNCs illustrates that the Au NRs (red arrow) are present as a core in the center of Cu_2O NPs (blue arrow) and the size of the CSNPs is nearly 145 nm (Figure 2b), well-matched with the AFM image (Figure 1b). Moreover, the pure graphene oxide sheet exists as a wrinkled 2D structure with layers (green arrows), as shown in Figure 2c. The AuNRs@Cu_2O/rGO nanocomposite clearly indicates the rGO wrapped (green arrow) around the AuNRs@Cu_2O CSNCs (Figure 2d). EDS analysis was performed to confirm the elemental distribution in the AuNRs@Cu_2O/rGO nanocomposite. As shown in Figure 2e, the AuNRs@Cu_2O/rGO nanocomposite consists of C, O, Cu, and Au elements. Further, the high-angle annular dark-field (HAADF) and the scanning TEM (STEM)-EDS elemental mapping of the AuNRs@Cu_2O/rGO nanocomposite indicate that the Au NR is fully covered with the Cu_2O particles as a shell (Figure 3). The elemental mapping shows violet, green, cyan, and red attributed to Cu, Au, carbon, and oxygen elements, respectively.

The phase purity of pure GO and AuNRs@Cu_2O/rGO nanocomposites was analyzed using the X-ray diffraction (XRD) pattern shown in Figure 4i,ii. A sharp peak at 2θ value of around 25.5° is observed for rGO (black line), which corresponds to the characteristic peak of the (002) plane, and graphene (001) was not observed; this is probably because GO was reduced to rGO and more functional groups were removed from the GO surface.[32] However, for the as-synthesized nanocomposite, the typical diffraction peak of reduced graphene oxide is observed at (002) plane (red). In addition, the diffraction peaks of Cu_2O at 2θ values of 29.7, 36.4, 42.4, 52.4, 61.5, 73.8, and 77.6 indexed to the planes of (110), (111), (200), (211), (220), (311), and (222), respectively, were attributed to the cubic phase of Cu_2O (PDF No. 01-1172) and small peaks at 38.2, 44.7, 64.7, and 77.5 were attributed to (111), (200), (220) (blue), and (311) of Au particles, which confirms the formation of AuNRs@Cu_2O/rGO. Moreover, the intensities of the Au peaks were

https://dx.doi.org/10.1021/acsomega.0c03487
ACS Omega 2020, 5, 24799−24810

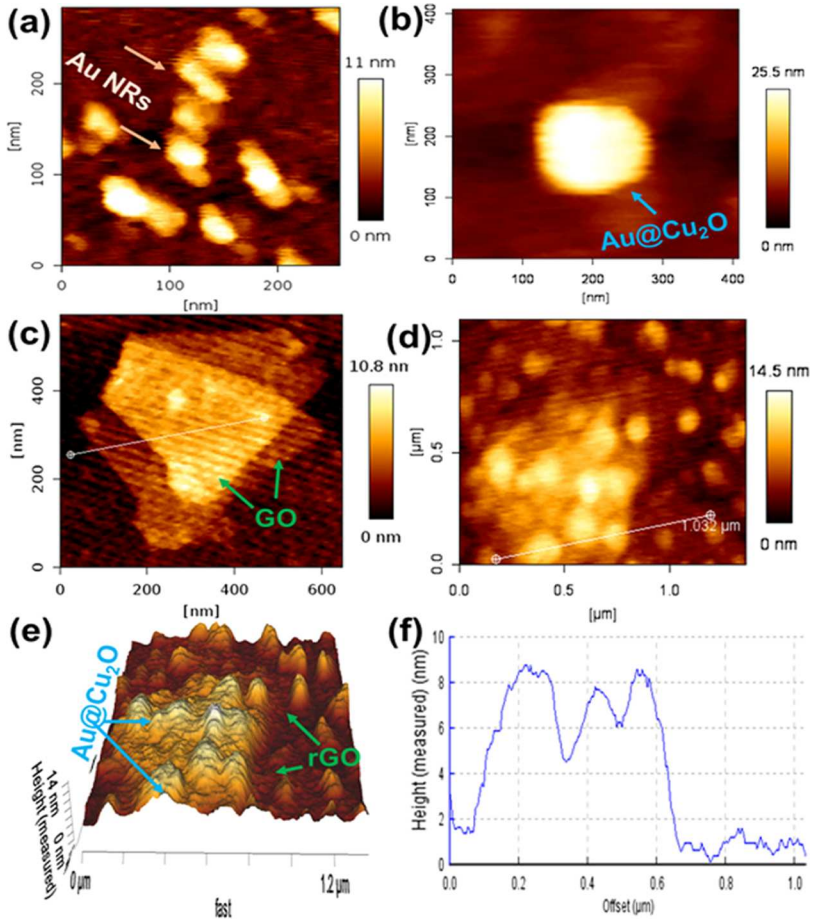

Figure 1. AFM images of (a) AuNRs, (b) AuNRs@Cu_2O CSNC, (c) GO, (d, e) AFM and 3D AFM images of the AuNRs@Cu_2O/rGO nanocomposite, and (f) height histogram profile of the AuNRs@Cu_2O/rGO nanocomposite.

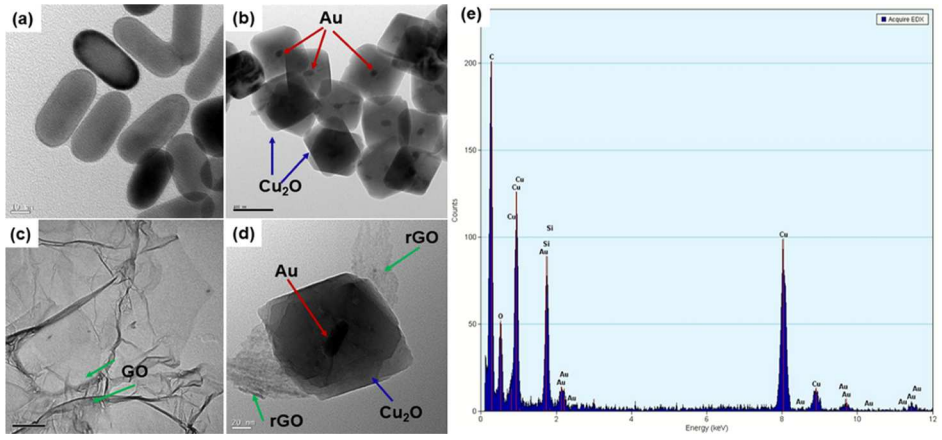

Figure 2. TEM images of (a) AuNRs, (b) AuNRs@Cu_2O CSNCs, and (c) GO and (d, e) TEM image and EDS spectra of the AuNRs@Cu_2O/rGO nanocomposite, respectively.

weaker than those of the Cu_2O peaks, indicating the presence of a Cu_2O shell and Au core in the composite.[33]

The effective reduction of GO to rGO and the formation of the AuNRs@Cu_2O/rGO nanocomposite can be further demonstrated by Fourier-transform infrared (FT-IR) and Raman spectroscopies. The FT-IR spectrum of GO (Figure 5i) shows that the peaks at 3463, 2450, 1734, 1640, 1383, and 1058 cm^{-1} were attributed to the stretching vibration of the O−H, C═O carbonyl, aromatic −C═C, and −C−O groups.[34] However, in the case of the AuNRs@Cu_2O/rGO nanocomposite, the peak intensities of all oxygenated groups gradually decreased, which indicates that GO was successfully converted into reduced graphene oxide (rGO). The peak intensity at 1631 cm^{-1} is increased, which indicates increasing −C═C moiety. Moreover, two new peaks appeared at 626 and 532 cm^{-1}, which corresponds to the Cu−O stretching vibration of the Cu_2O phase and Au.[35]

This result was further confirmed using Raman and XPS analyses. The Raman spectrum of the AuNRs@Cu_2O/rGO nanocomposite (Figure 5b) shows two bands at 1337 cm^{-1} (D

https://dx.doi.org/10.1021/acsomega.0c03487
ACS Omega 2020, 5, 24799−24810

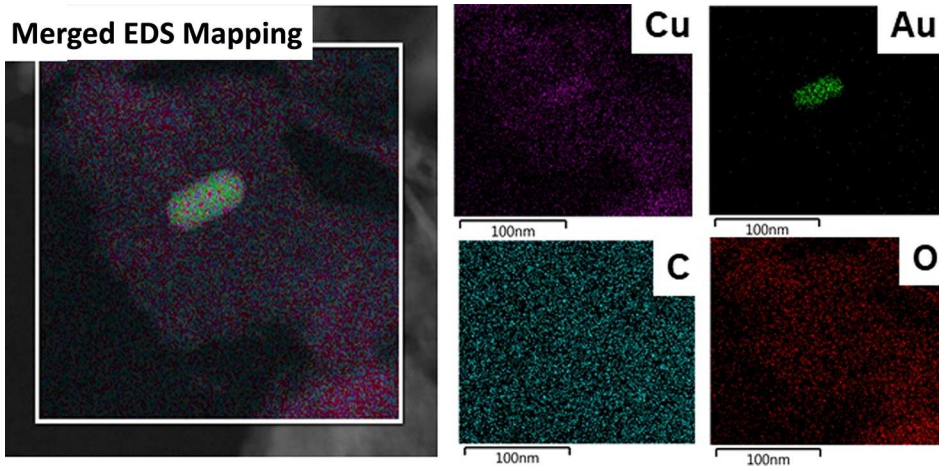

Figure 3. AuNRs@Cu_2O/rGO nanocomposite high-angle annular dark-field (HAADF) image along with elemental mapping images of Cu, Au, C, and O of individual particles.

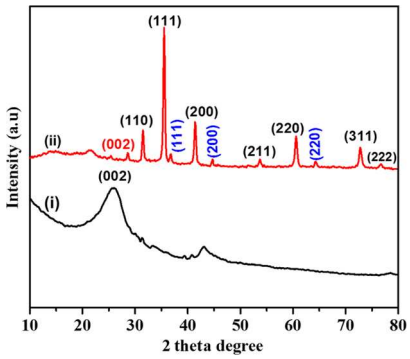

Figure 4. XRD patterns of (i) GO and (ii) AuNRs@Cu_2O/rGO nanocomposite.

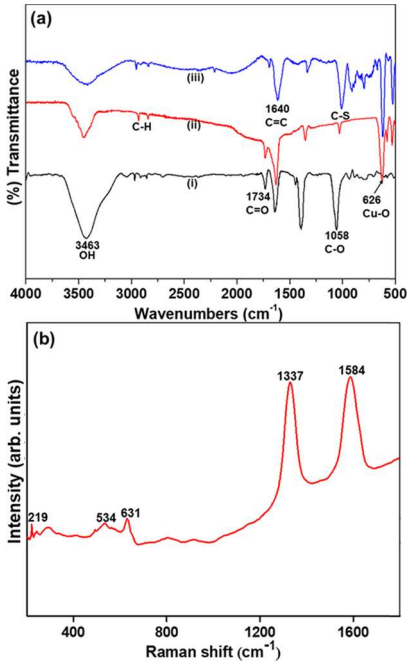

Figure 5. (a) FT-IR spectra of (i) GO and (ii, iii) AuNRs@Cu_2O/rGO nanocomposite before and after adsorption of MB dye and (b) Raman spectra of the AuNRs@Cu_2O/rGO nanocomposite.

band) and 1584 cm^{-1} (G band), which are the characteristic peaks of rGO structures.[36] Moreover, three peaks at 219, 534, and 631 cm^{-1}appeared, which are attributed to the Cu_2O phase.[37] In addition, a weak peak appeared at 489 cm^{-1} ascribed to Au particles.[38] The results clearly indicate the successful formation of the AuNRs@Cu_2O/rGO nanocomposite.

The X-ray photoelectron spectroscopy (XPS) measurements were performed for further confirmation of AuNRs@Cu_2O/rGO composite formation. The survey scan spectra of the AuNRs@Cu_2O/rGO nanocomposite (Figure 6ai) show the main peaks at 84, 280, 530, 932, and 952 eV attributed to the binding energies of Au 4f, C 1s, O 1s, and Cu 2p. The deconvolution spectrum of Cu 2p (Figure 6b) shows peaks at 932.4 and 952.1 eV corresponding to the binding energies of Cu 2p 3/2 and Cu 2p 1/2 of Cu(I), respectively. Moreover, the absence of a shake-up satellite peak at 945 eV indicates the absence of Cu(II). Thus, it is confirmed that Cu(I) is predominant in the AuNRs@Cu_2O/rGO nanocomposite. The AuNRs@Cu_2O/rGO nanocomposite was further characterized by ultraviolet−visible (UV−vis) absorption spectra. The UV−visible absorption spectra show (Figure S1) that the peaks at 521 and ∼754 nm are the characteristic surface plasmon resonance band of Au NRs,[38] whereas a broad peak at 690 nm is a Cu_2O characteristic peak.[22] Moreover, the peak at around 285 nm indicates the presence of the reduced form of graphene oxide rather than GO.

The adsorption capacity mainly depends on the surface area of the material. The specific surface areas of GO and AuNRs@Cu_2O/rGO nanocomposites were examined using isothermal N_2 adsorption−desorption analysis at 77 K. Compared to the isothermal curves between GO and AuNRs@Cu_2O/rGO nanocomposites, the extent of gas absorption is greatly enhanced in the nanocomposite. The Brunauer−Emmett−Teller (BET) surface areas of bare GO and AuNRs@Cu_2O/rGO nanocomposites are 9.7 and 205.5 m^2/g, respectively, presented in Figure 7i,ii. The average pore size is 3.5 nm, calculated using density functional theory (DFT) pore size distribution, and their size distribution is shown in the inset (Figure 7). This result clearly reveals that the AuNRs@Cu_2O/rGO nanocomposites show a mesoporous character. The high surface area of the AuNRs@Cu_2O/rGO nanocomposite may be due to the incorporation of AuNRs@Cu_2O CSNCs, which

https://dx.doi.org/10.1021/acsomega.0c03487
ACS Omega 2020, 5, 24799−24810

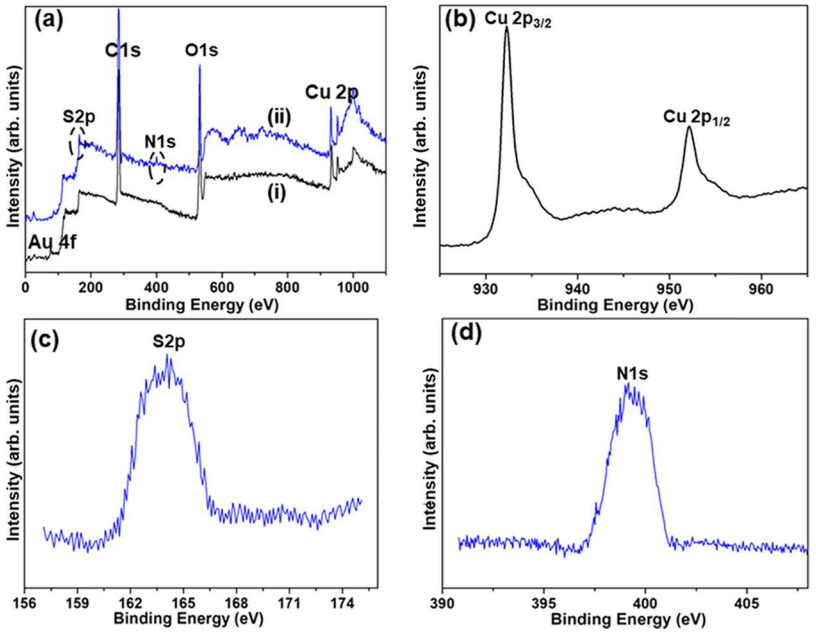

Figure 6. (a) Survey scan XPS spectra of (i, ii) AuNRs@Cu_2O/rGO nanocomposite before and after adsorption of MB dye, respectively, and (b, c) high-resolution XPS spectra of Cu 2p, S 2p, and N 1s.

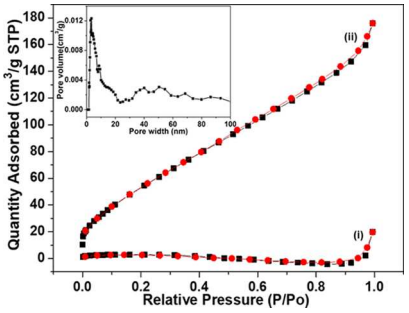

Figure 7. (i, ii) N_2 adsorption−desorption isotherms of pure GO and the AuNRs@Cu_2O/rGO nanocomposite.

increases the nanogaps around the nanoparticles and suppresses stacking and bundling of rGO, which influence the pore size and increase the surface area as well as the mesoporous nature compared with pure GO (microporous).[33] Moreover, based on single-point adsorption, the total pore volume of the AuNRs@Cu_2O/rGO nanocomposite was calculated to be 0.2723 cm^3/g at P/P_0 = 0.9937. This high mesoporous surface area plays a key role in the removal of methylene blue. In addition, after MB adsorption, the surface area of the AuNRs@Cu_2O/rGO nanocomposite was decreased from 205.5 to 102.002 m^2/g (Figure S2). After MB adsorption, the pores of the composite are occupied by the MB molecules, which limits pore accessibility of the composite. The above XPS, FT-IR, SEM, and BET results confirm the successful adsorption of MB by the AuNRs@Cu_2O/rGO nanocomposite.

Effect of pH on MB Adsorption. In a solution, the adsorption ability of the adsorbent mainly depends on the pH value. This could play a key role between the surface chemistry of the dye and the AuNRs@Cu_2O/rGO nanocomposite. The effect of pH on MB dye removal was studied in the pH range from 2 to 11. The solution pH was optimized using 0.1 M HCl/NaOH. The batch adsorption process was carried out by fixing the adsorbent dosage at 20 mg and the contact time was 30 min at a temperature of 298 K with a concentration of the MB dye of 0.02 g/L. The maximum removal efficiency >99% was observed at pH 10.5 and the minimum at pH 2, as shown in Figure 8i. The lowest adsorption at low pH is due to the

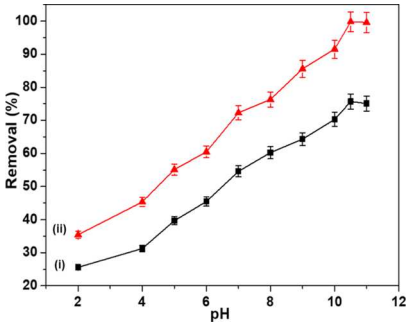

Figure 8. (i, ii) Effect of pH on the adsorption of MB dye by bare GO and the AuNRs@Cu_2O/rGO nanocomposite.

competition between the cationic dye molecules and protons, which leads to electrostatic repulsion between the adsorbate and adsorbent. At higher pH values, the surface of the AuNRs@Cu_2O/rGO nanocomposite becomes negatively charged and develops enhanced electrostatic attraction with positively charged dye molecules, which facilitates the adsorption of MB onto the AuNRs@Cu_2O/rGO nanocomposite. This demonstrates that the adsorption is primarily dependent on the pH of the solution. However, an increase in the solution pH beyond 10.5 ensured that saturation was reached. This might be due to the nonavailability of adsorption sites. In addition, the removal efficiency of GO was found to be 65%, as shown in Figure 8i. The high removal efficiency of the AuNRs@Cu_2O/rGO nanocomposite is mainly due to the high surface area, which is caused by the addition of Au NRs@Cu_2O CSNCs.

Effect of Time and Mechanism Study. The equilibrium adsorption time is an important parameter in the batch adsorption process. The effect of time on the adsorption of the

https://dx.doi.org/10.1021/acsomega.0c03487
ACS Omega 2020, 5, 24799−24810

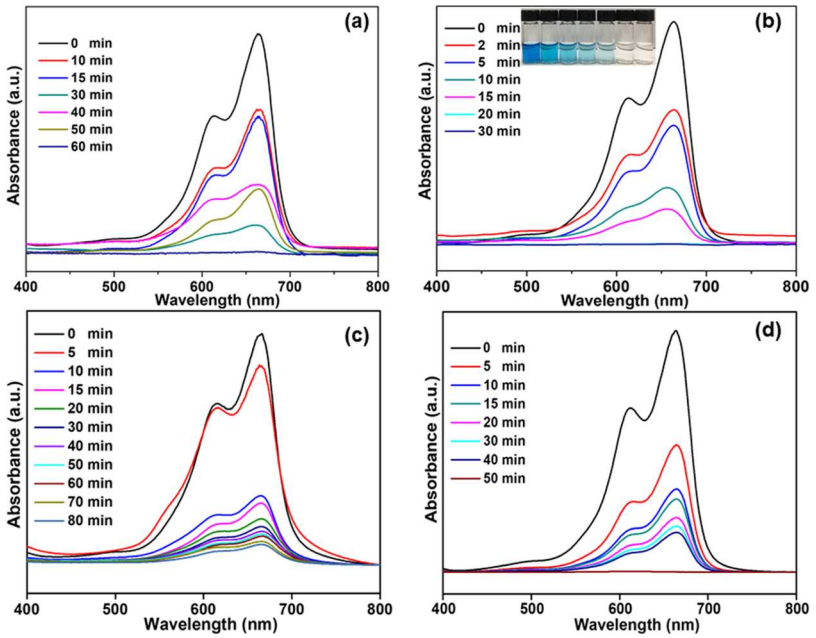

Figure 9. Time dependence of MB dye adsorption of (a) pure GO, (b) AuNRs@Cu_2O/rGO nanocomposite, (c) AuNRs@Cu_2O, and (d) Cu_2O/rGO.

dye was studied by maintaining constant the initial concentration of the MB dye at 298 K, with the dosage of 20 mg of bare GO and the AuNRs@Cu_2O/rGO nanocomposite. The adsorption of the dye increased with an increase in time and reached saturation at 60 min for GO, as shown in Figure 9a, whereas Figure 9b shows the time-dependent adsorption of the AuNRs@Cu_2O/rGO nanocomposite. The adsorbent reached saturation within 20 min. Due to the large surface area of the adsorbent, more available active sites and additional AuNRs@Cu_2O CSNCs boost the adsorption of dye molecules via enhancing the surface area and the porous nature of the adsorbent. For comparison, we have also analyzed the adsorption capacities of AuNRs@Cu_2O CSNCs and Cu_2O@rGO nanocomposite, as shown in Figure 9c,d. The AuNRs@Cu_2O CSNPs show an incomplete adsorption process even at 80 min, whereas the adsorption of the dye increased with an increase in time and reached saturation at 50 min for Cu_2O@rGO nanocomposite. The above results illustrate that the AuNRs@Cu_2O-embedded rGO nanocomposite significantly improved the removal of MB dye. In this ternary composite system, the AuNRs@Cu_2O CSNPs suppress stacking and bundling of rGO, leading to the high specific surface area with enormous sp^2 carbon bonds, and functional groups facilitate the removal of the dye via hydrogen bonds and $\pi-\pi$ electrostatic interactions. Importantly, the noble metal Au NRs boost the reactivity of Cu_2O in the composite, which may increase the rate of reaction and lead to the adsorption of MB dye reaching equilibrium within 20 min.[39,40]

To explore the possible mechanism between the adsorbent and adsorbate, we have used FT-IR and XPS techniques. The FT-IR spectra before and after the adsorption of MB dye are shown in Figure 5aiii. The peak at 3445 cm^{-1} corresponds to −OH of the AuNRs@Cu_2O/rGO nanocomposite. However, after adsorption of MB dye, the −OH peak shifted to 3332 cm^{-1}, representing the hydrogen bond interaction between the adsorbent and the MB dye. The intensity of the −C═O peak at 1728 cm^{-1} was decreased and shifted to 1706 cm^{-1}, which indicates the strong electrostatic attraction between the anionic form of −C═O (acid) of the adsorbent and the MB dye. In addition, the peak at 1631 cm^{-1} shifted to 1619 cm^{-1} is assigned to the $\pi-\pi$ interaction of the adsorbent and the adsorbate. Further, XPS analysis was carried out for the AuNRs@Cu_2O/rGO nanocomposite after MB dye removal (Figure 6ii). Compared to the peaks of Au 4f, C 1s, O 1s, and Cu 2p in the AuNRs@Cu_2O/rGO nanocomposite before adsorption, after removal of the MB dye, the AuNRs@Cu_2O/rGO nanocomposite shows additional peaks at 164 and 400 eV attributed to the binding energies of (Figure 6c) S 2p and (Figure 6d) N 1s, respectively, which indicates that MB is adsorbed on the structure of the AuNRs@Cu_2O/rGO nanocomposite.[41] The above results clearly confirm the adsorbate molecules of MB dye adsorbed onto the surface of the AuNRs@Cu_2O/rGO nanocomposite adsorbent. Further, the morphology of the composite does not change before and after MB removal, as seen in the SEM image in Figure S3a,b, which indicates a strong interfacial contact between the rGO and Au@Cu_2O core−shell NPs. The schematic representation of the mechanism is shown in Scheme 2.

Effect of Dosage and Concentration. The effect of adsorbent dosage on MB is shown in Figure S4i,ii. The adsorbent (AuNRs@Cu_2O/rGO) amount varied from 2 to 20 mg at an initial MB dye concentration of 0.02 g/L. From the results, it is noticed that the synthesized AuNRs@Cu_2O/rGO nanocomposite exhibited maximum removal efficiency of >99%, as shown in Figure S4ii, at a dosage of 20 mg, whereas GO shows only an adsorption efficiency of 62%, as shown in Figure S4i. While increasing the adsorbent dosage, the number of active sites increases. Thus, it could be concluded that the rate of adsorption increases and reaches the maximum adsorption at a constant dye concentration. Moreover, with further increases in the quantity of adsorbent, the percentage of adsorption does not change. This might be due to the limited transportation of MB dye ions to the active adsorption sites. In addition, the effect of the initial MB dye concentration on adsorption experiments were performed by preparing

https://dx.doi.org/10.1021/acsomega.0c03487
ACS Omega 2020, 5, 24799−24810

Scheme 2. Various Types of Interactions Involved in the Adsorption of Methylene Blue on the AuNRs@Cu_2O/rGO Nanocomposite

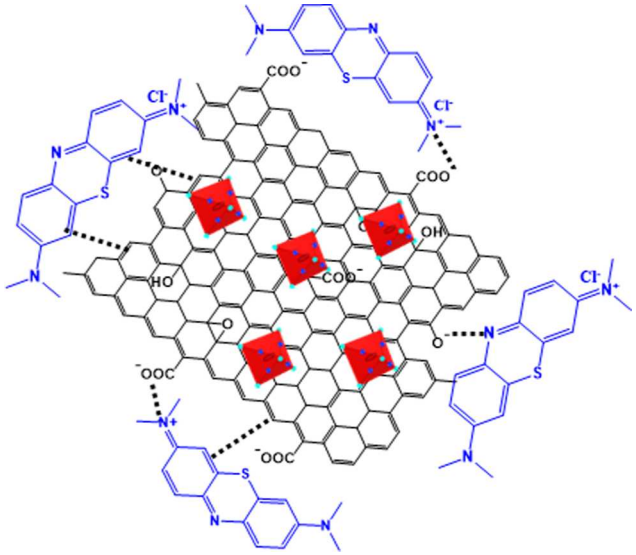

various concentrations from 0.02 to 0.2 g/L. The removal efficiency of MB onto the adsorbent was decreased with increasing dye concentration. The removal efficiency was decreased from 99 to 48% for the AuNRs@Cu_2O/rGO nanocomposite, as shown in Figure S5ii, and 62 to 16% for GO, as shown in Figure S5i. This is because, at a lower concentration, a large surface area of the adsorbent is available for the adsorption of dye ions. At higher concentrations, due to the saturation of the active sites of the adsorbent, the degree of adsorption is decreased.

Adsorption Isotherm Studies. Typical isotherm models were employed to understand the interaction between the adsorbate and the adsorbent at equilibrium and the maximum adsorption capacity of the adsorbent at 298 K. Among all of the isotherm models, Langmuir and Freundlich's models are commonly used. The Langmuir adsorption isotherm is used to attain a maximum adsorption capacity formed from the complete monolayer coverage of the adsorbent surface. The linear form of the Langmuir equation can be addressed as

$$\frac{C_e}{q_e} = \frac{C_e}{q_m} + \frac{1}{q_m b} \quad (1)$$

where C_e is the equilibrium concentration (mg/L), q_e is the amount of dye ion adsorbed at equilibrium (mg/g), q_m is the maximum adsorption capacity of the adsorbent (mg/g), and b is the equilibrium constant related to the adsorption energy. A plot of C_e/q_e vs C_e is used to calculate q_m and b values from the slope and intercepts of the plots.

The Freundlich isothermal can be applied for the determination of metal ions on the multilayer surface and the linear form is expressed as

$$\log\ q_e = \log k_f + \frac{1}{n} \log C_e \quad (2)$$

where k_f (mg/g) and n are the Freundlich constants indicating the capacity of the adsorbent for the adsorbate and the strength of the adsorption, respectively. Figure 10a illustrates a good linear fit of the Langmuir isotherm model with the correlation coefficient value (R^2 = 0.9971). The maximum MB adsorption capacity (243.9 mg/g) and other parameters are shown in Table 1. However, Figure 10b shows the linear fit of the Freundlich model with the correlation coefficient value (R^2 = 0.9308). Moreover, both models are well fit; nevertheless, based on the correlation coefficient values, the adsorption data were well fitted for Langmuir rather than the Freundlich isotherm model. The calculated n value is 4.17, calculated from the Freundlich isotherm model, which indicates that the adsorption process is favorable.[42,43] In addition, a dimensionless parameter R_L derived from the Langmuir isotherm is described by the following equation

$$R_L = \frac{1}{1 + bC_i} \quad (3)$$

where C_i (mg/g) is the initial concentration of the dye and b is the Langmuir constant. As per the literature, the value of R_L lies between 0 and 1 for favorable adsorption, while $R_L > 1$ represents unfavorable adsorption and $R_L = 1$ represents linear adsorption.[44] The calculated R_L value was 0.032, which indicates that the adsorption of MB on the AuNRs@Cu_2O/rGO nanocomposite is favorable. This developed model indicates that an adsorbent surface has a specific number of sites where the adsorbate molecules can be adsorbed and involves monolayer adsorption. Moreover, the adsorption capacity of the developed AuNRs@Cu_2O/rGO nanocomposite is compared with those of the materials reported in Table 2. It clearly indicates that the developed adsorbent is one of the best adsorbents, as shown in comparison in Table 2.[45−54]

Adsorption Kinetics and Thermodynamic Studies. The rate of adsorption is important for the batch adsorption process. For MB adsorption, the following pseudo-first-order and pseudo-second-order models were tested.[55,56]

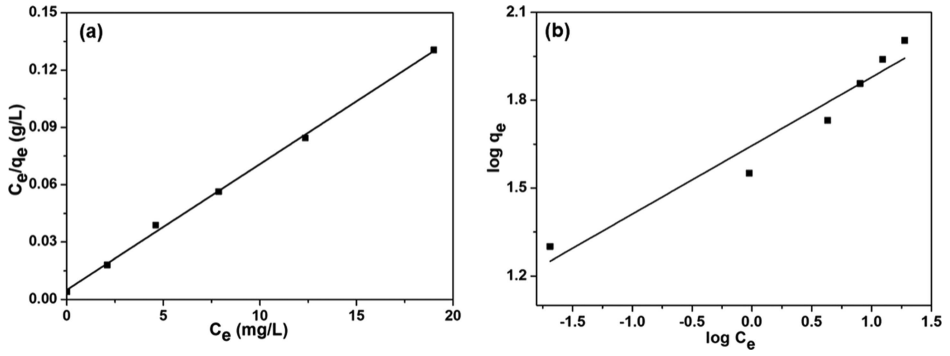

Figure 10. Fit of data for MB dye adsorption on the AuNRs@Cu_2O/rGO nanocomposite: (a) Langmuir and (b) Freundlich isotherms at 298 K.

https://dx.doi.org/10.1021/acsomega.0c03487
ACS Omega 2020, 5, 24799−24810

Table 1. Langmuir and Freundlich Parameters for Adsorption of MB Dye on the AuNRs@Cu_2O/rGO Nanocomposite

	Langmuir			Freundlich		
temperature (K)	q_m (mg/g)	b (L/g)	R^2	K_f (mg/g)	n	R^2
298	243.97	1.518	0.9971	44.157	4.278	0.9308
308	123.45	2.667	0.9946	40.504	3.512	0.9222
318	107.52	1.107	0.9930	38.185	3.137	0.9189

Table 2. Comparison of MB Adsorption Capacity of the AuNRs@Cu_2O/rGO Nanocomposite with those of Various Adsorbents

adsorbent type	capacity (mg/g)	removal (%)	time (min)	refs
AC alginate	230.0	98.9	1200	45
CuO/MCM$_4$1	87.8	96.4	60	46
Fe_3O_4@Ag/SiO_2	128.5	99.6	50	47
mixed Ti, Al, and Si oxides	162.9		30	48
GO/CA	181.8	92.7	420	49
garlic straw	256.4	87.0	200	50
HKUST-1/GO	183.4	>90	30	51
brown macroalga	95.4	96.9	120	52
Fe_3O_4@AMCA-MIL-53(Al) nanocomposite	325.62	94.6	210	53
NH_2-MWCNTs@Fe_3O_4	178.5		60	54
AuNRs@Cu_2O/rGO	243.9	99.8	20	this work

The linear form of the pseudo-first-order kinetic model is as follows

$$\log(q_e - q_t) = \log q_e - \frac{k_1 t}{2.303} \quad (4)$$

The linear form of the pseudo-second-order kinetic model is as follows

$$\frac{t}{q_t} = \frac{1}{k_2 q_e^2} + \left(\frac{1}{q_e}\right) t \quad (5)$$

where K_1 (0.1070 g/(mg min)) and K_2 (0.0154 g/(mg min)) are the rate constants of the pseudo-first-order and pseudo-second-order kinetic models determined from the slope of the plot of $\log(q_e - q_t)$ vs t and t/q_t vs t, respectively. The correlation coefficient (R^2) values of the pseudo-first-order and pseudo-second-order kinetic models are $R^2 = 0.8303$ and $R^2 = 0.9984$, respectively. The value of R^2 for the pseudo-first-order is very low compared to that of the pseudo-second-order kinetic model. Therefore, the adsorption on the synthesized composite is followed by pseudo-second-order kinetics (Figure S6).

The temperature-dependent adsorption process is associated with several thermodynamic parameters such as Gibbs free energy (ΔG), enthalpy change (ΔH), and entropy change (ΔS) where the Van't Hoff equation is as follows

$$\ln K_c = \frac{\Delta S}{R} - \frac{\Delta H}{RT} \quad (6)$$

$$\Delta G = -RT \ln K_c \quad (7)$$

where T is the temperature, R is the universal gas constant (8.314 J/(mol K)), and K is obtained from the Langmuir constants b and q_m.

The values of ΔH and ΔS were calculated from the slope and the intercept of the plot of $\ln K_c$ vs $1/T$, respectively (Figure S7). All of the obtained thermodynamic parameters are listed in Table S1. The value of ΔG is negative, which confirms that the adsorption process is spontaneous and thermodynamically favorable. The negative value of ΔH suggested that the adsorption process is exothermic, which is also supported by the decreasing adsorption of MB with increasing temperature. The positive value of ΔS is assigned to the AuNRs@Cu_2O/rGO nanocomposite for MB and the increased disorder at the solid–liquid interface during the adsorption process.[57]

Reusability of the Composite. Reusability is the most important key factor in economic efficiency. After the isotherm studies, the reusability of the composite was studied to evaluate its efficiency. The regeneration and reuse of the as-prepared AuNRs@Cu_2O/rGO nanocomposite were investigated by washing the adsorbent thrice in an acidic medium and DI water. The recycling efficiency of the adsorbent was evaluated under optimized adsorption conditions (pH 10.5, initial concentration of 20 mg/L at 298 K). Figure S8 shows that it is clear that even after five adsorption cycles, the dye removal efficiency decreased from 99 to 86%. Our study shows that the as-prepared AuNRs@Cu_2O/rGO nanocomposite exhibits a very fast dye removal capability with 99.8% of the removal within 20 min.

CONCLUSIONS

In this work, we prepared a novel composite material comprising AuNR@Cu_2O core–shell nanoparticles and rGO via a simple synthetic route. The AuNRs@Cu_2O/rGO nanocomposite showed superior stability, mainly owing to the strong intercalation bonding between rGO and Au@Cu_2O core–shell nanoparticles. The structure and morphology of the composite were characterized by AFM and TEM analysis, demonstrating the AuNRs (40 nm) doped with Cu_2O (~145 nm) nanoparticles wrapped by wrinkled 2D-rGO. It should be noted that the AuNRs@Cu_2O/rGO nanocomposite showed better MB removal efficiency in aqueous solutions than the Au@Cu_2O CSNCs or GO because of specific surface area and the mesoporous character. The N_2 gas sorption analysis proved that the surface area of the composite was significantly increased (205.5 m^2/g) compared to that of pristine GO (9.7 m^2/g). The adsorption equilibrium for MB dye onto the composite was in good agreement with Langmuir adsorption isotherm with an excellent dye sorption capacity (243.9 mg/g). Additional parameters affecting MB removal, including pH, contact time, temperature, initial dye concentration, and adsorbent dosage, were investigated. The thermodynamic parameters (ΔG, ΔH, and ΔS) reveal that the adsorption process is spontaneous and favorable. Moreover, Au NR-doped Cu_2O particles in the composite act as an additive by increasing the specific surface area and suppressing rGO stacking, leading to very fast saturation of adsorption in 20 min with 99% removal efficiency. Furthermore, these studies demonstrate that AuNRs@Cu_2O/rGO heterogeneous nanocomposite is a promising material for various fields, such as catalysis and electrochemical applications.

https://dx.doi.org/10.1021/acsomega.0c03487
ACS Omega 2020, 5, 24799–24810

EXPERIMENTAL SECTION

Materials and Chemicals. Gold(III) chloride trihydrate ($HAuCl_4{\cdot}3H_2O$, 99.9%), $AgNO_3$ (99%), cetyltrimethylammonium bromide (CTAB (99%)), sodium borohydride ($NaBH_4$ (99%)), ascorbic acid (AA (>99 %)), NaOH (96%), copper nitrate trihydrate ($Cu(NO_3)_2{\cdot}3H_2O$), sodium dodecyl sulfate (SDS (95%)), graphite powder, hydrogen peroxide (H_2O_2, 30 wt %), hydrochloric acid (HCl, 36.0−38.0 wt %), sulfuric acid (H_2SO_4, 95−98 wt %), potassium permanganate ($KMnO_4$), hydrazinium hydrate ($N_2H_4{\cdot}H_2O$, 85%), methyl blue (MB), and ethanol (C_2H_5OH, >99.7 wt %) were obtained from Sigma-Aldrich. Ultrapure deionized water (DI; Continental Water Systems) was used for the preparation of all of the solutions and in all of the experiments. The glassware was cleaned and washed with DI water.

Preparation of Au Seed Solution. The seed solution was prepared based on our earlier report.[31] Briefly, 0.25 mL of an aqueous solution of $HAuCl_4{\cdot}3H_2O$ (0.01 M) was poured into 7.5 mL of a 0.10 M CTAB solution in a glass test tube and stirred for a while until a very bright brown-yellow color appeared. Subsequently, 0.6 mL of an aqueous 0.01 M ice-cold $NaBH_4$ solution was added, followed by stirring, and the color of the solution changed to pale brown-yellow. Then, the test tube was kept in an incubator maintained at 28 °C for 3 h.

Synthesis of Au Nanorods. Briefly, 400 μL of 0.01 M $HAuCl_4{\cdot}3H_2O$ was added dropwise to 9.5 mL of 0.1 M CTAB and stirred. Further, 30 μL of 0.01 M $AgNO_3$ solution was added, and the color of the solution appeared to be bright brown-yellow. To this, a reducing agent of 0.064 mL of 0.1 M AA was added and the solution became colorless. Finally, 0.01 mL of the as-prepared gold seed solution was added under gentle stirring at room temperature. The color of the solution gradually changed to blue within 5 min, and the total solution was incubated at 28 °C overnight. Then, this solution was washed with water twice to remove excess CTAB.

Synthesis of AuNRs@Cu_2O Core−Shell Nanocubes. Typically, 0.125 g of sodium dodecyl sulfate was added to 80 mL of copper nitrate trihydrate ($Cu(NO_3)_2{\cdot}3H_2O$) aqueous solution (0.003 M). Subsequently, 4.0 mL of the as-prepared Au NR solution was added dropwise, followed by the addition of 10 mL of 0.4 M NaOH solution. Then, the mixture was rapidly stirred for 15 min at room temperature. To this, 10 mL of the AA solution (0.04 M) was added dropwise with vigorous stirring. Then, the color of the solution changed from blue to yellowish-green, indicating the formation of AuNRs@Cu_2O CSNCs. Finally, the resulting solution was centrifuged at 7000 rpm and washed thrice with water and ethanol.

Synthesis of AuNRs@Cu_2O/rGO Nanocomposites. The AuNRs@Cu_2O/rGO nanocomposites were prepared by a simple reduction process using $N_2H_4{\cdot}H_2O$. The above synthesized AuNRs@Cu_2O core−shell nanocubes (0.50 g) were dispersed in 50 mL of water and an aqueous solution of GO (0.5 mg/mL, 3 mL) was added under vigorous stirring for 15 min. Subsequently, $N_2H_4{\cdot}H_2O$ (1 mL, 0.5 M) was added dropwise to the suspension with constant stirring for 1 h. The final material was separated by centrifugation and washed thrice with ethanol and distilled water to remove residual ions and N_2H_4. In the end, the as-prepared solids were dried for 4 h in a vacuum oven at 60 °C and stored for further experiments. The detailed schematic representation of the formation of the composite is shown in Scheme 1.

Adsorption Studies. To study the adsorption behavior of the AuNRs@Cu_2O/rGO nanocomposites, batch adsorption experiments were carried out. Typically, various concentrations of MB solution (0.02, 0.04, 0.06, 0.08, 0.10, and 0.20 g/L) were prepared from the stock solution (1.0 g/L). Briefly, 20 mg of AuNRs@Cu_2O/rGO adsorbent was added into a 250 mL conical flask containing 100 mL of the above MB solution and stirred for 30 min in an open environment at 298 K. The dye solution pH was adjusted using HCl/NaOH (0.10 M). Then, the solution was removed from the adsorbent by filtration and centrifugation. The absorbance of the initial and final residual concentrations of MB was monitored at 664 nm (max) using a UV−vis spectrophotometer. The percentage removal and adsorption capacity of MB were calculated using the following equations[58]

$$\text{dye removal (\%)} = \frac{(C_o - C_e)}{C_o} \times 100 \tag{8}$$

$$\text{adsorption capacity } q_e = \frac{(C_o - C_e)V}{M} \tag{9}$$

where C_o (mg/L) and C_e (mg/L) are the initial and equilibrium concentrations of the dye solution, respectively, and q_e is the equilibrium dye adsorption capacity. V (L) and M (mg) are the volumes of the solution and dosage, respectively. Moreover, the adsorption kinetic study was carried out at a fixed time (2 to 30 min) with an adsorbent dose of 2 mg and an initial MB concentration of 0.02 g/L at pH 10.5. In addition, to understand the temperature's effect, the adsorption of the materials at various temperatures (298, 308, and 318 K) was measured using a temperature-controlled stirrer.

Characterization. The morphological and size characterization was determined using a JEOL JEM-ARM 200F series TEM instrument. Element mapping and selected-area electron diffraction (SAED) patterns were obtained with an accelerating voltage of 300 kV and a camera constant of 28 mmA (Tecnai G2). Atomic force microscopy (AFM) was performed with a JPK NanoWizard II bioatomic force microscopy in contact mode to determine the surface morphology. The phase purity of the synthesized composite was determined using a Rigaku Ultima III X-ray diffractometer equipped with a Cu sealed tube (λ = 1.541 Å). The following conditions were applied: 40 kV, 30 mA, increase = 0.05°, and scan speed = 3°/min. The composite functional groups were illustrated using FT-IR with a Thermo Nicolet iS-10 spectrometer using a KBr pellet in transmission mode and Raman spectroscopy using a Micro Raman system (Ramboss 500 i), He-Ne laser beam at 633 nm, and 1800 lines per mm grating with 50 X objective lens at room temperature. The detailed composition of the AuNRs@Cu_2O/rGO nanocomposite was analyzed using a Thermo Scientific K-Alpha$^+$ (XPS) system equipped with a 100−4000 eV range of motion, a 180° double-focusing hemispherical analyzer with a 128-channel detector, and Al Kα microfocused X-ray source. The UV−vis spectra were measured using a Varian Cary 100 UV−vis spectrophotometer for the analysis of the dye removal concentration. The pore diameter and specific surface area of the composite materials were calculated from a N_2 adsorption isotherm measured using Micromeritics ASAP-2020; high-purity N_2 gas (99.999%) was used for the measurements. A scanning electron microscope (SEM, S-4700, Hitachi, Japan) with an accelerating voltage of 20 kV was used for further morphological analysis of the composite.

https://dx.doi.org/10.1021/acsomega.0c03487
ACS Omega 2020, 5, 24799−24810

■ ASSOCIATED CONTENT

Supporting Information

The Supporting Information is available free of charge at https://pubs.acs.org/doi/10.1021/acsomega.0c03487.

Material characterization; UV−vis absorbance spectroscopy; BET; SEM; effect of dosage; effect of concentration; kinetics; thermodynamics; recycle study (PDF)

■ AUTHOR INFORMATION

Corresponding Authors

Venkateswarlu Sada − *Department of Nanochemistry, Gachon University, Seongnam 13120, Republic of Korea; Department of Chemistry, Kyungpook National University, Daegu 41566, Republic of Korea;* orcid.org/0000-0001-7042-6937; Email: venkisada67@gmail.com

Minyoung Yoon − *Department of Chemistry and Green-Nano Materials Research Center, Kyungpook National University, Daegu 41566, Republic of Korea;* orcid.org/0000-0001-7436-6273; Email: myyoon@knu.ac.kr

Kyusik Yun − *Department of Bionanotechnology, Gachon University, Seongnam 13120, Republic of Korea;* Email: ykusik@gachon.ac.kr

Authors

Hansa Mahajan − *Department of Nanochemistry and Department of Bionanotechnology, Gachon University, Seongnam 13120, Republic of Korea*

Shiva Kumar Arumugasamy − *Department of Bionanotechnology, Gachon University, Seongnam 13120, Republic of Korea;* orcid.org/0000-0001-5213-7314

Atanu Panda − *Department of Nanochemistry, Gachon University, Seongnam 13120, Republic of Korea; Department of Chemistry, Kyungpook National University, Daegu 41566, Republic of Korea;* orcid.org/0000-0003-4049-3885

Complete contact information is available at: https://pubs.acs.org/10.1021/acsomega.0c03487

Author Contributions

The manuscript was written through the contributions of all authors. All authors have given approval to the final version of the manuscript.

Notes

The authors declare no competing financial interest.

■ ACKNOWLEDGMENTS

This research was supported by the National Research Foundation of Korea (NRF) grant funded by the Ministry of Science and ICT (NRF-2017R1C1B5076834 and NRF-2019R1F1A1060715).

■ ABBREVIATIONS USED

AFM, atomic force microscopy; BET, Brunauer−Emmett−Teller; CSNCs, core−shell nanocubes; FT-IR, Fourier-transform infrared; HADF-STEM, high-angle annular dark-field-scanning transmission electron microscopy; MB, methyl blue; NRs, nanorods; rGO, reduced graphene oxide; SEM, scanning transmission electron microscopy; TEM, transmission electron microscopy; UV, ultraviolet; XRD, X-ray diffraction

■ REFERENCES

(1) Das, R.; Vecitis, C. D.; Schulze, A.; Cao, B.; Ismail, A. F.; Lu, X.; Chen, J.; Ramakrishna, S. Recent Advances in Nanomaterials for Water Protection and Monitoring. *Chem. Soc. Rev.* **2017**, *46*, 6946−7020.

(2) Mon, M.; Bruno, R.; Ferrando-Soria, J.; Armentano, D.; Pardo, E. Metal−Organic Framework Technologies for Water Remediation: Towards a Sustainable Ecosystem. *J. Mater. Chem. A* **2018**, *6*, 4912−4947.

(3) Wang, Z.; Zhang, J. H.; Jiang, J. J.; Wang, H. P.; Wei, Z. W.; Zhu, X.; Pan, M.; Su, C. Y. A Stable Metal Cluster-Metalloporphyrin MOF With High Capacity for Cationic Dye Removal. *J. Mater. Chem. A* **2018**, *6*, 17698−17705.

(4) Yan, H.; Tao, X.; Yang, Z.; Li, K.; Yang, H.; Li, A.; Cheng, R. Effects of the Oxidation Degree of Graphene Oxide on the Adsorption of Methylene Blue. *J. Hazard. Mater.* **2014**, *268*, 191−198.

(5) Ravula, S.; Larm, N. E.; Liu, Y.; Atwood, J. L.; Baker, S. N.; Baker, G. A. Ionothermal Synthesis of Magnetically-Retrievable Mesoporous Carbons from Alkyne-Appended Ionic Liquids and Demonstration of Their use in Selective Dye Removal. *New J. Chem.* **2018**, *42*, 1979−1986.

(6) Fan, L.; Luo, C.; Sun, M.; Li, X.; Lu, F.; Qiu, H. Preparation of Novel Magnetic Chitosan/Graphene Oxide Composite as Effective Adsorbents Toward Methylene Blue. *Bioresour. Technol.* **2012**, *114*, 703−706.

(7) He, K.; Zeng, G.; Chen, A.; Huang, Z.; Peng, M.; Huang, T.; Chen, G. Graphene Hybridized Polydopamine-Kaolin Composite as Effective Adsorbent for Methylene Blue Removal. *Composites, Part B* **2019**, *161*, 141−149.

(8) Vikrant, K.; Giri, B. S.; Raza, N.; Roy, K.; Kim, K. H.; Rai, B. N.; Singh, R. S. Recent Advancements in Bioremediation of Dye: Current Status and Challenges. *Bioresour. Technol.* **2018**, *253*, 355−367.

(9) Hassan, M. M.; Carr, C. M. A Critical Review on Recent Advancements of the Removal of Reactive Dyes from Dye House Effluent by Ion-Exchange Adsorbents. *Chemosphere* **2018**, *209*, 201−219.

(10) Chen, W.; Mo, J.; Du, X.; Zhang, Z.; Zhang, W. Biomimetic Dynamic Membrane for Aquatic Dye Removal. *Water Res.* **2019**, *151*, 243−251.

(11) Rachuri, Y.; Subhagan, S.; Parmar, B.; Bisht, K. K.; Suresh, E. Selective and Reversible Adsorption of Cationic Dyes by Mixed Ligand Zn (II) Coordination Polymers Synthesized by Reactant Ratio Modulation. *Dalton Trans.* **2018**, *47*, 898−908.

(12) Ngulube, T.; Gumbo, J. R.; Masindi, V.; Maity, A. An Update on Synthetic Dyes Adsorption onto Clay Based Minerals: A State-of-Art Review. *J. Environ. Manage.* **2017**, *191*, 35−57.

(13) Du, P. Y.; Li, H.; Fu, X.; Gu, W.; Liu, X. A 1D Anionic Lanthanide Coordination Polymer as an Adsorbent Material for the Selective Uptake of Cationic Dyes from Aqueous Solutions. *Dalton Trans.* **2015**, *44*, 13752−13759.

(14) Huang, Q.; Song, S.; Chen, Z.; Hu, B.; Chen, J.; Wang, X. Biochar-Based Materials and their Applications in Removal of Organic Contaminants from Wastewater: State of the Art Review. *Biochar* **2019**, *1*, 45−73.

(15) Naushad, M.; ALOthman, Z. A.; Awual, M. R.; Alfadul, S. M.; Ahamad, T. Adsorption of Rose Bengal Dye from Aqueous Solution by Amberlite Ira-938 Resin: Kinetics, Isotherms, and Thermodynamic Studies. *Desalin. Water Treat.* **2016**, *57*, 13527−13533.

(16) Sharma, G.; Naushad, M.; Pathania, D.; Mittal, A.; El-desoky, G. E. Modification of Hibiscus Cannabinus Fiber by Graft Copolymerization: Application for Dye Removal. *Desalin. Water Treat.* **2015**, *54*, 3114−3121.

(17) Kim, S.; Lee, J.; Son, Y.; Yoon, M. Study of the Dye Adsorption Kinetics of Metal−Organic Frameworks in Aqueous Media. *Bull. Korean Chem. Soc.* **2020**, *41*, 843−850.

(18) Liu, Y.; Yang, Z. H.; Song, P. P.; Xu, R.; Wang, H. Facile Synthesis of $Bi_2MoO_6/ZnSnO_3$ Heterojunction with Enhanced Visible Light Photocatalytic Degradation of Methylene Blue. *Appl. Surf. Sci.* **2018**, *430*, 561−570.

(19) Banerjee, S.; Benjwal, P.; Singh, M.; Kar, K. K. Graphene Oxide (rGO)-Metal Oxide (TiO_2/Fe_3O_4) Based Nanocomposites for the Removal of Methylene Blue. *Appl. Surf. Sci.* **2018**, *439*, 560−568.

(20) Tan, K. B.; Vakili, M.; Horri, B. A.; Poh, P. E.; Abdullah, A. Z.; Salamatinia, B. Adsorption of Dyes by Nanomaterials: Recent Developments and Adsorption Mechanisms. *Sep. Purif. Technol.* **2015**, *150*, 229−242.
(21) Ghaedi, A. M.; Vafaei, A. Applications of Artificial Neural Networks for Adsorption Removal of Dyes from Aqueous Solution: A Review. *Adv. Colloid Interface Sci.* **2017**, *245*, 20−39.
(22) Li, X.; Zhang, Y.; Jing, L.; He, X. Novel N-doped CNTs Stabilized Cu_2O Nanoparticles as Adsorbent for Enhancing Removal of Malachite Green and Tetrabromobisphenol. *Chem. Eng. J.* **2016**, *292*, 326−339.
(23) Xu, Y.; Liu, P.; Cao, Y.; Sun, Y.; Zhang, G. Room-temperature Synthesis of Cu_2O Nanostructures and Their Morphology-dependent Adsorption Properties. *Bull. Korean Chem. Soc.* **2016**, *37*, 1114−1123.
(24) Xiong, L.; Li, S.; Zhang, B.; Du, Y.; Miao, P.; Ma, Y.; Han, Y.; Zhao, H.; Xu, P. Galvanic Replacement-Mediated Synthesis of Hollow Cu_2O−Au Nanocomposites and Au Nanocages for Catalytic and SERS Applications. *RSC Adv.* **2015**, *5*, 76101−76106.
(25) Oh, J. T.; Chowdhury, S. R.; Lee, T.; Misra, M. Synergetic Influence of Au/Cu_2O Core-Shells Nanoparticle on Optical, Photo-Electrochemical, and Catalytic Activities of Au/Cu_2O/TiO_2 Nanocomposite. *Dyes Pigm.* **2019**, *160*, 936−943.
(26) Zhang, W.; Wang, B.; Hao, C.; Liang, Y.; Shi, H.; Ao, L.; Wang, W. Au/Cu_2O Schottky Contact Heterostructures with Enhanced Photocatalytic Activity in Dye Decomposition and Photoelectrochemical Water Splitting Under Visible Light Irradiation. *J. Alloys Compd.* **2016**, *684*, 445−452.
(27) Liao, H.; Wang, Z. Adsorption Removal of Amaranth by Nanoparticles-Composed Cu_2O Microspheres. *J. Alloys Compd.* **2018**, *769*, 1088−1095.
(28) Kyzas, G. Z.; Deliyanni, E. A.; Bikiaris, D. N.; Mitropoulos, A. C. Graphene Composites as Dye Adsorbents. *Chem. Eng. Res. Des.* **2018**, *129*, 75−88.
(29) Papageorgiou, D. G.; Kinloch, I. A.; Young, R. J. Mechanical Properties of Graphene and Graphene-Based Nanocomposite. *Prog. Mater. Sci.* **2017**, *90*, 75−127.
(30) Parvathi, V. P.; Parimaladevi, R.; Sathe, V.; Umadevi, M. Environmental Photochemistry by Plasmonic Semiconductor Decorated GO Nanocomposites: SERS Detection and Visible Light Driven Degradation of Aromatic Dyes. *Appl. Surf. Sci.* **2019**, *473*, 864−872.
(31) Liang, X.; Govindaraju, S.; Yun, K. Dual Applicability of Polyaniline Coated Gold Nanorods: A Study of Antibacterial and Redox Activity. *BioChip J.* **2018**, *12*, 137−145.
(32) Venu, M.; Venkateswarlu, S.; Reddy, Y. V.; Seshadri Reddy, A.; Gupta, V. K.; Yoon, M.; Madhavi, G. Highly Sensitive Electrochemical Sensor for Anticancer Drug by a Zirconia Nanoparticle-Decorated Reduced Graphene Oxide Nanocomposite. *ACS Omega* **2018**, *3*, 14597−14605.
(33) Yuan, G.; Lu, M.; Fei, J.; Guo, J.; Wang, Z. Morphologically Controllable Synthesis of Core−Shell Structured Au@Cu_2O with Enhanced Photocatalytic Activity. *RSC Adv.* **2015**, *5*, 71559−71564.
(34) Naushad, Mu.; Ahamad, T.; Maswari, B. M. Al.; Alqadami, A. A.; Alshehri, S. M. Nickel Ferrite Bearing Nitrogen-Doped Mesoporous Carbon as Efficient Adsorbent for the Removal of Highly Toxic Metal ion From Aqueous Medium. *Chem. Eng. J.* **2017**, *330*, 1351−1360.
(35) Li, X.; Zhang, Y.; Jing, L.; He, X. Novel N-Doped CNTs Stabilized Cu_2O Nanoparticles as Adsorbent for Enhancing Removal of Malachite Green and Tetrabromobisphenol A. *Chem. Eng. J.* **2016**, *292*, 326−339.
(36) Wang, A.; Yu, W.; Huang, Z.; Zhou, F.; Song, J.; Song, Y.; Long, L.; Cifuentes, M. P.; Humphrey, M. G.; Zhang, L.; Shao, J.; et al. Covalent Functionalization of Reduced Graphene Oxide with Porphyrin by Means of Diazonium Chemistry for Nonlinear Optical Performance. *Sci. Rep.* **2016**, *6*, No. 23325.
(37) Deng, Y.; Handoko, A. D.; Du, Y.; Xi, S.; Yeo, B. S. In Situ Raman Spectroscopy of Copper and Copper Oxide Surfaces During Electrochemical Oxygen Evolution Reaction: Identification of CuIII Oxides as Catalytically Active Species. *ACS Catal.* **2016**, *6*, 2473−2481.
(38) Ma, Y.; Zhu, Y.; Liu, B.; Quan, G.; Cui, L. Colorimetric Determination of Hypochlorite Based on the Oxidative Leaching of Gold Nanorods. *Materials* **2018**, *11*, 1629.
(39) Zheng, L.; Yu, H.; Yue, Y.; Wu, F.; He, Y. Visual Chronometric Assay for Chromium (III) ions Based on the Cu_2O Nanocube-Mediated Clock Reaction. *ACS Appl. Mater. Interfaces* **2017**, *9*, 11798−11802.
(40) Ray, C.; Dutta, S.; Sarkar, S.; Sahoo, R.; Roy, A.; Pal, T. A Facile Synthesis of 1D Nano Structured Selenium and Au Decorated Nano Selenium: Catalysts for the Clock Reaction. *RSC Adv.* **2013**, *3*, 24313−24320.
(41) Hu, T.; Liu, Q.; Gao, T.; Dong, K.; Wei, G.; Yao, J. Facile Preparation of Tannic Acid−Poly (vinyl alcohol)/Sodium Alginate Hydrogel Beads for Methylene Blue Removal from Simulated Solution. *ACS Omega* **2018**, *3*, 7523−7531.
(42) Venkateswarlu, S.; Yoon, M. Core-Shell Ferromagnetic Nanorod Based on Amine Polymer Composite (Fe_3O_4@DAPF) for Fast Removal of Pb (II) from Aqueous Solutions. *ACS Appl. Mater. Interfaces* **2015**, *7*, 25362−25372.
(43) Venkateswarlu, S.; Yoon, M. Surfactant-Free Green Synthesis of Fe_3O_4 Nanoparticles Capped with 3, 4-Dihydroxyphenethylcarbamodithioate: Stable Recyclable Magnetic Nanoparticles for the Rapid and Efficient Removal of Hg (II) ions from Water. *Dalton Trans.* **2015**, *44*, 18427−18437.
(44) Albadarin, A. B.; Collins, M. N.; Naushad, Mu.; Shirazian, S.; Walker, G.; Mangwandi, C. Activated Lignin-Chitosan Extruded Blends for Efficient Adsorption of Methylene Blue. *Chem. Eng. J.* **2017**, *307*, 264−272.
(45) Nasrullah, A.; Bhat, A. H.; Naeem, A.; Isa, M. H.; Danish, M. High Surface Area Mesoporous Activated Carbon-Alginate Beads for Efficient Removal of Methylene Blue. *Int. J. Biol. Macromol.* **2018**, *107*, 1792−1799.
(46) Liang, Z.; Zhao, Z.; Sun, T.; Shi, W.; Cui, F. Enhanced Adsorption of the Cationic Dyes in the Spherical CuO/Meso-Silica Nano Composite and Impact of Solution Chemistry. *J. Colloid Interface Sci.* **2017**, *485*, 192−200.
(47) Saini, J.; Garg, V. K.; Gupta, R. K. Removal of Methylene Blue from Aqueous Solution by Fe_3O_4@Ag/SiO_2 Nanospheres: Synthesis, Characterization and Adsorption Performance. *J. Mol. Liq.* **2018**, *250*, 413−422.
(48) Pal, U.; Sandoval, A.; Madrid, S. I.; Corro, G.; Sharma, V.; Mohanty, P. Mixed Titanium, Silicon, and Aluminum Oxide Nanostructures as Novel Adsorbent for Removal of Rhodamine 6G and Methylene Blue as Cationic Dyes from Aqueous Solution. *Chemosphere* **2016**, *163*, 142−152.
(49) Li, Y.; Du, Q.; Liu, T.; Sun, J.; Wang, Y.; Wu, S.; Wang, Z.; Xia, Y.; Xia, L. Methylene Blue Adsorption on Graphene Oxide/Calcium Alginate Composites. *Carbohydr. Polym.* **2013**, *95*, 501−507.
(50) Kallel, F.; Chaari, F.; Bouaziz, F.; Bettaieb, F.; Ghorbel, R.; Chaabouni, S. E. Sorption and Desorption Characteristics for the Removal of a Toxic Dye, Methylene Blue from Aqueous Solution by a Low Cost Agricultural by-Product. *J. Mol. Liq.* **2016**, *219*, 279−288.
(51) Li, L.; Liu, X. L.; Geng, H. Y.; Hu, B.; Song, G. W.; Xu, Z. S. A MOF/Graphite Oxide Hybrid (MOF: HKUST-1) Material for the Adsorption of Methylene Blue from Aqueous Solution. *J. Mater. Chem. A* **2013**, *1*, 10292−10299.
(52) Daneshvar, E.; Vazirzadeh, A.; Niazi, A.; Koush, M.; Naushad, Mu.; Bhatnagar, A. Desorption of Methylene Blue dye From Brown Macroalga: Effects of Operating Parameters, Isotherm Study and Kinetic Modeling. *J. Cleaner Prod.* **2017**, *152*, 443−453.
(53) Alqadami, A. A.; Naushad, Mu.; Alothman, Z. A.; Ahamad, T. Adsorptive Performance of MOF Nanocomposite for Methylene Blue and Malachite Green Dyes: Kinetics, Isotherm and Mechanism. *J. Environ. Manage.* **2018**, *223*, 29−36.
(54) Ahamad, T.; Naushad, Mu.; Eldesoky, G. E.; Saeedi, S. I. Al.; Nafady, A.; Kadhi, N. S. Al.; Muhtaseb, A. H. Al.; Khan, A. A.; Khan, A. Effective and Fast Adsorptive Removal of Toxic Cationic Dye

https://dx.doi.org/10.1021/acsomega.0c03487
ACS Omega 2020, 5, 24799−24810

(MB) From Aqueous Medium Using Amino-Functionalized Magnetic Multiwall Carbon Nanotubes. *J. Mol. Liq.* **2019**, *282*, 154−161.
(55) Alqadami, A. A.; Naushad, Mu.; Abdalla, M. A.; Ahamad, T.; Alothman, Z. A.; Alshehri, S. M.; Ghfar, A. A. Efficient Removal of Toxic Metal Ions from Waste Water Using a Recyclable Nano-composite: A Study of Adsorption Parameters and Interaction Mechanism. *J. Cleaner Prod.* **2017**, *156*, 426−436.
(56) Alqadami, A. A.; Naushad, Mu.; Alothman, Z. A.; Ghfar, A. A. Novel Metal−Organic Framework (MOF) Based Composite Material for the Sequestration of U(VI) and Th(IV) Metal Ions From Aqueous Environment. *ACS Appl. Mater. Interfaces* **2017**, *9*, 36026−36037.
(57) Naushad, M. Surfactant Assisted Nano-Composite Cation Exchanger: Development, Characterization and Applications for the Removal of Toxic Pb^{2+} from Aqueous Medium. *Chem. Eng. J.* **2014**, *235*, 100−108.
(58) Liang, C.; Ren, J.; Hankari, S. E.; Huo, J. Aqueous Synthesis of a Mesoporous Zr-Based Coordination Polymer for Removal of Organic Dyes. *ACS Omega* **2020**, *5*, 603−609.

https://dx.doi.org/10.1021/acsomega.0c03487
ACS Omega 2020, 5, 24799−24810